Chalcogenide Letters Vol. 15, No. 4, April 2018, p. 207 - 218

EFFECT OF Mn DOPING ON STRUCTURAL, OPTICAL AND MAGNETIC PROPERTIES OF CdS DILUTED MAGNETIC SEMICONDUCTOR NANOPARTICLES

A. GADALLA, M. ALMOKHTAR, A. N. ABOUELKHIR*
Physics Department, Faculty of Science, Assiut University, Egypt

Manganese doped cadmium sulfide diluted Magnetic Semiconductor nanoparticles (CdS:Mn) NPs have been prepared by wet chemical precipitation method at different Mn weight percentages (0, 2, 4, 6, 8, and 10%). Mercaptoethanol is the capping agent that used to form the nanostructure and prevent the aggregations of the particles. The structure properties of the obtained nanoparticles have been studied using x- ray diffraction pattern. Energy dispersive x-ray carried out to specify the chemical composition of the prepared nanoparticles. The optical properties have been determined by analysis of UV-vis and PL spectra. Vibrating sample magnetometer (VSM) technique used to identify the magnetic properties of the samples. The crystal size estimated from (XRD) of the prepared NPs was around ~ (4 - 7) nm with cubic zinc blende structure. EDX spectroscopy was used to confirm the incorporation of Mn at CdS lattice. The energy band gap of the nanoparticles has been estimated using UV-Vis spectroscopy. VSM data of Mn doped CdS nanoparticles show weak hysteresis loops at room temperature which indicating the change from diamagnetic of undoped CdS to superparamagnetic behavior of Mn doped CdS nanoparticles.

(Received February 5, 2018; Accepted April 19, 2018)

Keywords: CdS:Mn nanoparticle; Quantum dots; Optical spectra; HRTEM; X-rays; Diluted Magnetic Semiconductors.

1. Introduction

Nanomaterials can be defined as materials whose structural have dimensions in the range of 1 to 100 nm. Since 1990's, nanotechnology has become a subject in physics, chemistry, biology and medicine. Nanoparticles exhibit unique properties which different from bulk materials [1-3]. The change in the properties of NPs is caused mainly by two factors; the increase in the surface area to volume ratio and change in the electronic structure of the material due to the quantum effects with varying particle size. Diluted magnetic semiconductors are a semiconductor which doped by magnetic ions. These materials have many optical and magnetic properties. The most commonly used DMS are II–VI quantum dot semiconductors (CdSe , ZnS, CdS, etc.), doped with elements (e.g. Gd, Tb, Eu, Co, Mn, Fe) substituting their original host cations. The unique properties of these particles results from the interaction of the spin induced magnetic moment of the transition metal ions with the electronic bands of the host semiconductor lattice [4, 24]. In the present paper, wet chemical method has been used to synthesis undoped and Mn doped cadmium sulfide nanoparticles caped with mercaptoethanol. Effect of Mn doping on Structural, morphology, optical and magnetic properties has been studied in this paper.

*Corresponding author: aboelkhier@hotmail.com

2. Experimental Procedures

2.1. Materials

Cadmium Chloride ($CdCl_2$) 99.5 %, Sodium Sulphide Nonohydrate ($Na_2S.9H_2O$) 99%, Merceptoethenol (ME); (C_2H_5OSH) and Manganese Chloride ($MnCl_2$) 99% were obtained from Aldrich. All chemicals and solvents were used as received without additional purification. Undoped and Mn doped CdS nanocrystals prepared by wet chemical route method [3, 18]. Mercaptoethanol was used as capping agent for the synthesized nanoparticles.

2.2 Preparation of CdS Nanoparticles

The starting materials in their respective solvents were taken in a round-bottomed flask fitted with a reflex cooling tube. Then Aqueous solutions of ($CdCl_2$ - 0.01 M), ($Na_2S.9H_2O$ - 0.01 M) and (merceptoethenol 0.001 M) were prepared. Firstly, the aqueous solution of merceptoethenol was injected drop wise in the solution of $CdCl_2$ at the rate of 1 ml per minute. A magnetic stirrer with hot plate was used for stirring and refluxing the solution under Ar atmosphere at 100 ^{0}C for 2 h. There after 0.01 M solution of $Na_2S.9H_2O$ was injected drop wise into the solution. Subsequently yellow precipitate settled down in the bottom of the flask. The reaction can be determined in the following equation;

$$CdCl_2 + Na_2S9H_2O \longrightarrow CdS + 2NaCl + 9H_2O$$

The precipitate of CdS is insoluble in water and was thoroughly washed several times in double distilled water. The presence of mercaptoethanol prevents the particles to grow to a bigger size. The nanoparticles were collected from the reaction medium by centrifugation for 30 minute at 4000 rpm. Finally, the obtained product is dried in vacuum oven at 70 ^{0}C for 1 h.

2.3. Preparation of Mn Doped CdS Nanoparticle

The water used in the preparation was distilled, deoxygenated, and deionized. The deoxygenating was done by bubbling with argon gas. For doping, an aqueous solution of $MnCl_2$ was injected directly to the solution of $CdCl_2$ on the reaction flask and refluxed under Ar atmosphere at 100 ^{0}C for 2 h. There after 0.01 M solution of $Na_2S.9H_2O$ was injected drop wise into the solution. The reaction can be determined in the following equation;

$$(1 - x)\,CdC1_2 + xMnC1_2 + Na_2S9H_2O \longrightarrow Cd_{1-x}Mn_xS + 2NaCl + 9H_2O.$$

The weight percentage of Mn was fixed by varying x value to get Mn doped CdS NPs (2, 4, 6, 8, and 10 wt %). Samples were prepared by varying the volume of Mn precursor and keeping volumes sodium sulfide constant. The solution of the product samples was precipitated then washed several times with distilled water and dried in vacuum oven at 70 ^{0}C for 1h. Finally the dried powder was grounded. Ar gas and glove bag are very important and used to prevent Mn oxidation during the experimental. The as prepared samples; CdS and Mn doped CdS NPs (2, 4, 6, 8, & 10 wt %) were coded as S1, S2, S3, S4, S5, and S6 respectively.

3. Results and discussion

3.1. Energy Dispersive X-ray Spectroscopy (EDX) Analysis

The typical EDX spectra of undoped and Mn doped CdS NPs (2, 4, 6, 8, & 10 wt %) are shown in Figure1. The quantitative weight percentage of the compositional elements Cd, S and Mn in the prepared samples are shown in Table 1.

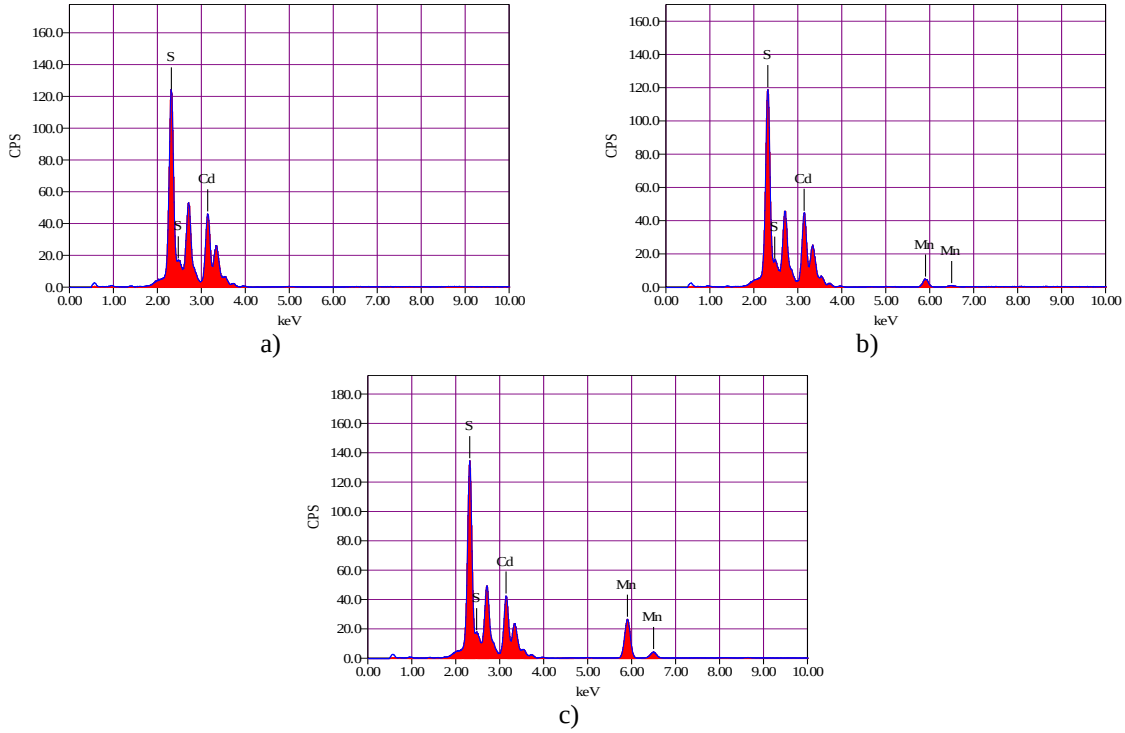

Fig. 1. Energy dispersive x- ray spectra (EDX) of a) CdS (b) CdS:Mn (2 wt %), (c) CdS:Mn (10 wt %).

Table 1. EDX compositional analysis of the prepared samples

S.Code	*As prepared samples*	*Elements from EDX analysis in wt %*		
		Mn	*Cd*	*S*
S1	CdS	0	79.06	20.94
S2	CdS:Mn (2 wt %)	1.87	75.55	22.58
S3	CdS:Mn (4 wt %)	3.69	74.2	22.11
S4	CdS:Mn (6 wt %)	5.49	72.6	21.91
S5	CdS:Mn (8 wt %)	7.38	70.43	22.19
S6	CdS:Mn (10 wt %)	9.46	68.71	21.83

The EDX spectrum of undoped and Mn doped CdS NPs indicates chemical purity of the samples. The strong peaks related to Cd, S and Mn are obtained in the spectrum. It clearly shows that the intensity of Mn peaks increases with the addition of Mn concentrations. The deviation of the estimated elements from the target elements were within acceptable limits and attributed to variations in compositional homogeneity. Therefore, the EDX spectra shows well agreement with the experimental Mn concentration used in synthesized NPs.

3.2. Structural and Morphology Characterization

Figure 2 displays diffraction pattern of undoped and Mn doped CdS NPs. X-ray diffraction (XRD) spectra were recorded at room temperature using Philips PW 1710 diffractometer with Cu-Kα radiation with λ = 1.5406 A° and diffraction angle 2θ from 10° to 90°. It was noticed that, there were three diffraction peaks in all the prepared samples at 2θ values near to 26.45, 43.88 and 51.97 degrees. The peaks are corresponding to the reflection from (111), (220) and (311) planes of the cubic phase of the CdS. The XRD pattern of the prepared NPs is perfectly equivalent to the standard cubic CdS (ICCD card No. 04-006-3897). No other phases related to impurities have been detected. The observed broadening of all diffraction peaks indicates that the products are in nanosize scale. The calculations of samples are reported in Table 2.

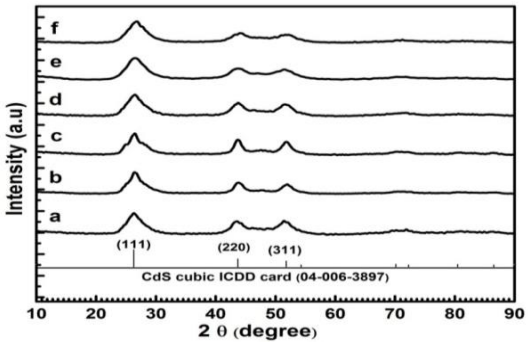

Fig. 2. XRD pattern of a) CdS (b) CdS:Mn (2 wt %), (c) CdS:Mn (4 wt %), (d) CdS:Mn (6 wt %), (e) CdS:Mn (8 wt %) and (f) CdS:Mn (10 wt %).

Table 2 XRD results for synthesized NPs.

Samp. code	*Samp. type*	*2Θ°*	*FWHM*	*(hkl)*	d_{111} *spacing*	*Av. Particle size (nm)*	*Lattice Parameter (a) (nm)*	*Cell volume* $(nm)^3$
S1	CdS	26.34	2.90	(111)	0.3386	7.2	0.586	0.2012
S2	CdS:Mn (2 wt %)	26.43	2.96	(111)	0.3369	6	0.583	0.1981
S3	CdS:Mn (4 wt %)	26.51	2.98	(111)	0.3359	5.5	0.581	0.1961
S4	CdS:Mn (6 wt %)	26.60	3.12	(111)	0.3348	4	0.579	0.1941
S5	CdS:Mn (8 wt %)	26.68	3.31	(111)	0.3338	4.4	0.578	0.1931
S6	CdS:Mn (10wt%)	26.68	3.40	(111)	0.3338	4	0.578	0.1931

The crystallite size of the samples was calculated from the three diffraction peaks by using the Sherrer equation [5, 21];

$$D = \frac{0.9\lambda}{\beta cos\theta} \tag{1}$$

where θ the Bragg diffraction angle, λis the x-ray wavelength and β the full width at half maximum (FWHM) of the peak. The particle size for undoped and Mn doped CdS NPs (2, 4, 6, 8, & 10 wt %) were found to be 7.2, 6, 5.5, 4, 4.4 and 4 nm respectively. XRD patterns show that there is no change in the phase upon the incorporation of Mn in the host CdS lattice. That can be explained according to Vegard's law; the dopant alone cannot generate an individual peak by the side of host peak but it can produce shift in the position of the host peak. In addition, the 2 θ position peaks is found at 26.34, 26.43, 26.51, 26.60, 26.68 and 26.68 degree showing slightly increasing shifts to the larger angles with the increment of the Mn concentration. The small shifts in the position of peaks confirm the incorporation of Mn^{+2} into the CdS lattice. The lattice parameter (a) of cubic zinc blende are calculated for the prepared NPs by using the Bragg's law ($2d_{hkl}Sin\theta = n\lambda$), where (θ) is the peak position, (λ) is the wavelength of X rays, (n) is the order of diffraction (usually n = 1) and (d_{hkl}) is the inter planer separation according to Miller indices hkl which defined from the next two equations [19]:

$$\frac{1}{d_{hkl}^2} = \frac{h^2+k^2+l^2}{a^2} \tag{2}$$

$$a = \frac{\lambda}{2\sin\theta}\sqrt{h^2+k^2+l^2} \tag{3}$$

It is important to notice that the unit cell lattice volume is decreasing considerably by increasing of Mn concentration; Table 2. This can be explained by the incorporation of smaller Mn^{+2} ions (0.92 A) replacing larger Cd^{+2} ions (0.97 A) in cubic host semiconducting CdS lattice structure [6]. The variation of lattice volumes of the Mn doped samples is shown in the Fig. 3.

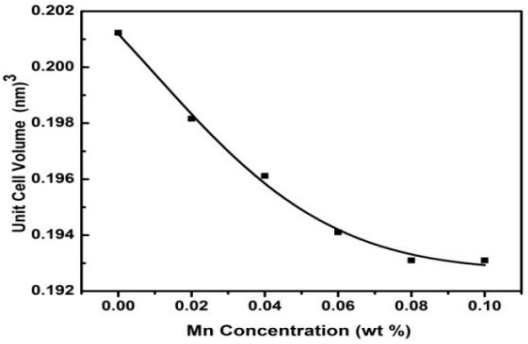

Fig. 3 Variation of unit cell volume $(nm)^3$ for undoped and Mn doped CdS NPs

The micrographs of nanocrystals were imaged by HRTEM JEM-2100 (JOEL) operated at 200 KV of accelerated voltage. For obtaining the HRTEM images, the prepared sample were dispersed in absolute chloroform ultrasonically and then the colloid was dropped on to Cu-grid coated with amorphous carbon film. HRTEM images and the corresponding size distribution diagrams of CdS and CdS:Mn NPs (4, 8 &10 wt %) are illustrated in figure 4, and so we can deduce that all the particles are nearly spherical and have different size distribution. The observed average particle size of the samples was estimated to be 7.99, 6.42, 5.6, and 4.5 nm, for pure and Mn doped CdS (4, 8 & 10 wt %) respectively. The obtained values of average crystallite size were estimated using histogram chart from different areas on the HRTEM grid. The particle size measured from the HRTEM analysis closely matched with the particle size that calculated from Scherrer method. HRTEM analysis also confirms the nanodimensional state of the synthesized NPs.

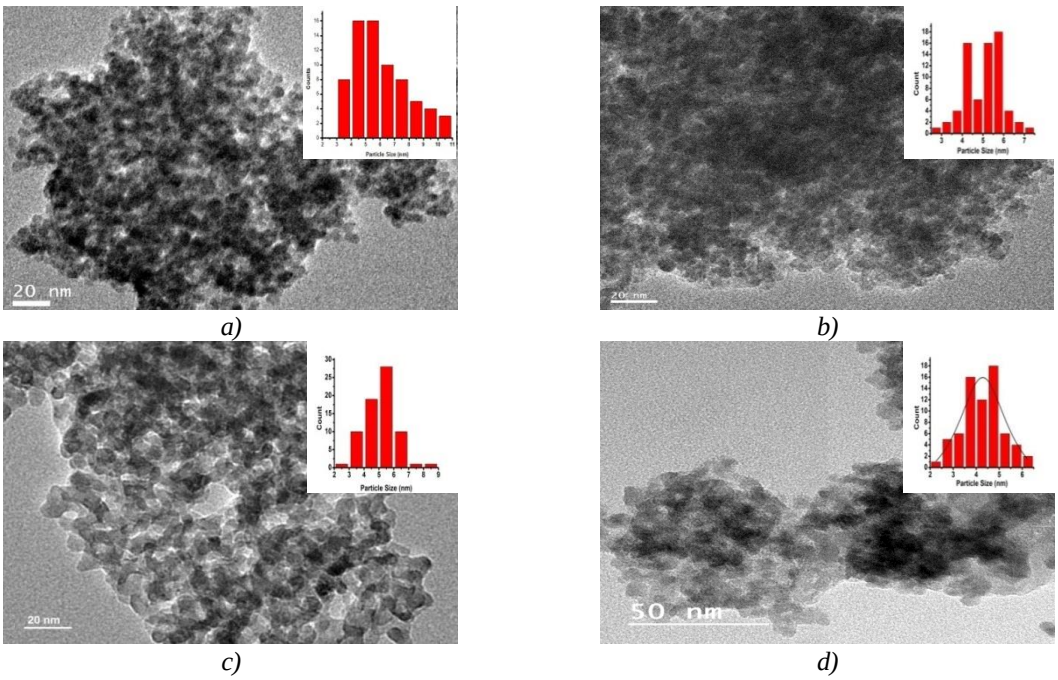

Fig. 4 High resolution TEM micrographs and histogram for a) CdS (b) CdS:Mn (4 wt %), (c) CdS:Mn (8 wt %) and (d) CdS:Mn (10 wt %).

It is noticed that, the particle size measured from HRTEM micrograph is larger than that value calculated from XRD. This might be explained by the fact that, X-ray diffraction results based on the mean size of sample obtained from XRD pattern which is smaller than that obtained from all the structural layers of sample when using HRTEM. Also in XRD method, system standard errors were not eliminated.

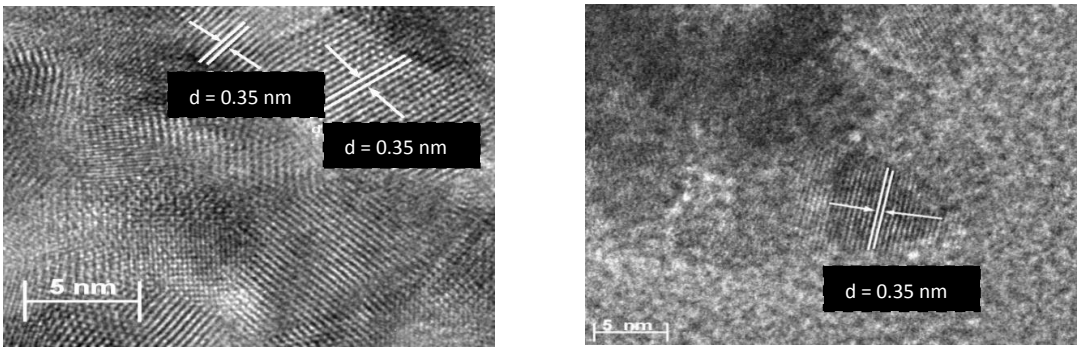

a) *b)*

Fig. 5. HRTEM micrographs of crystalline lattice fringes for a) undoped CdS and (b)CdS:Mn (10 wt %)

Figure 5 clearly revealing crystalline lattice fringes. The interplanar lattice spacing measured from the HRTEM micrographs was found to be around 0.35 nm, for undoped CdS, and Mn doped CdS (10 wt %). The observed interplanar lattice spacing value is corresponding to the (111) plane of the cubic phase of the prepared samples and closely agreed with the results of XRD.

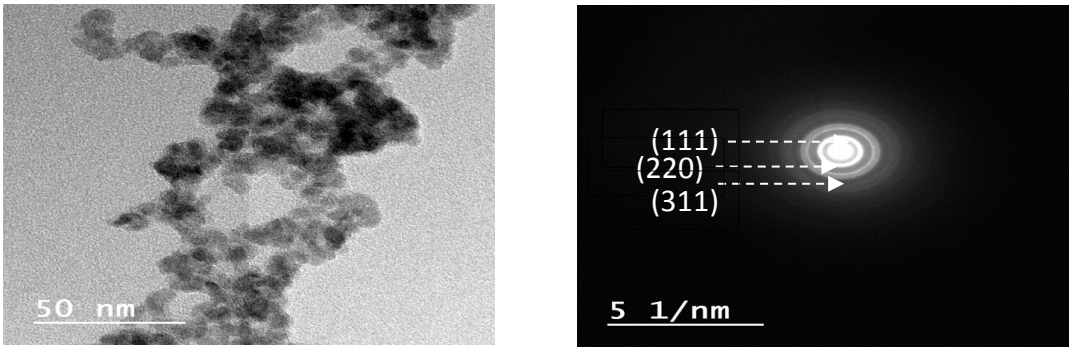

a) *b)*

Fig. 6. a) HRTEM image and b) (SAED) pattern of the undoed CdS sample

HRTEM image of the pure CdS NPs with selected area electron diffraction (SAED) pattern are shown in figure 6 which reveals the polycrystalline nature. The rings in the SAED pattern are indexed as (111), (220) and (311) planes of the cubic phase. The imaged interplanar lattice spacing (d) has been estimated from all diffraction rings using the next Eq. [21];

$$d = \lambda L/R \quad (4)$$

where, R is the distance from the central spot to the according ring, L is the camera length between specimen and the film and λ is the wavelength of the electron beam . The imaged interplanar lattice spacing values are found to be 0.33, 0.21, 0.17 nm corresponds to the (111), (220) and (311) planes respectively.

3.3. Optical Properties

UV-Vis Absorbance Characterization

Figure 7 represent UV- Vis absorption spectra of the prepared CdS:Mn NPs. the characteristic absorption edge of pure CdS are observed at 504 nm. Also, the absorption edge of doped NPs is blue shifted compared to the bulk (512 nm) and undoped NPs. This action results from quantum confinement effect [7, 22]. The optical absorption spectra of undoped and Mn doped CdS NPs (2, 4, 6, 8, & 10 wt %) shows absorption edge at 504, 477, 449, 435, 420 and 410 nm respectively. The blue shift from the spectra can be clearly observed in the figure with increasing Mn concentration.

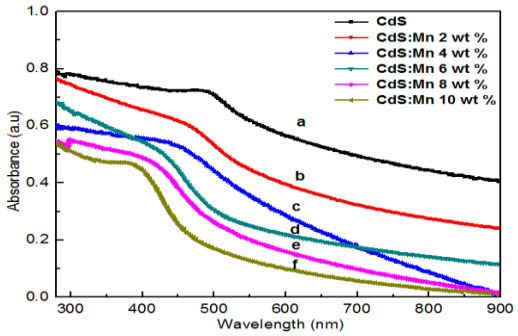

Fig. 7. UV-Vis absorbance spectra of a) CdS (b) CdS:Mn (2 wt %), (c) CdS:Mn (4 wt %), (d) CdS:Mn (6 wt %), (e) CdS:Mn (8 wt %) and (f) CdS:Mn (10 wt %).

The optical absorption coefficient (α) has been evaluated from the measured spectral, using Beer-Lambert law [25]:

$$\alpha = 2.303\ A/T \tag{5}$$

where (A) is the absorbance and (T) is and width of the sample`s cell (1cm). The optical band gap was calculated using Tauc`s relation [8]:

$$(\alpha h\nu)^{1/n} = (h\nu - Eg) \tag{6}$$

where, ($h\nu$) represents the photon energy, (α) is the absorption co efficient, (E_g) is the optical band gap of the nanoparticles , (A) is a constant, and the exponent (n) is depending to the type of transition. The exponent (n) is equal to half *and* two according to the direct and indirect allowed band gaps, respectively. The plot of $(\alpha h\nu)^2$ versus photon energy ($h\nu$) shown in Figure 8, is linear at absorption edge indicating a direct transition. The energy band gap is determined by extrapolating the straight line portion to energy axis at $(\alpha h\nu)^2$ equal zero. From Table 3, it is noticed that the energies value (E_g) is gradually increase by increasing of Mn concentration. The obtained (E_g) values of the pure and Mn doped CdS nanoparticles (2, 4, 6, 8, & 10 wt %) was found to be 2.5, 2.6, 3, 3.2, 3.1 and 3.4 eV, respectively. This behavior is resulted from the incorporation of Mn ions inside the CdS lattice structure [9, 21]. By using the calculated band gap values, the average particle size has been measured by the Brus formula [10];

$$E_{np} = E_g + \hbar\pi^2/2R^2\,[1/m_e^* + 1/m_h^*] - 1.8\ e^2/4\pi\varepsilon_0\,\varepsilon_r R \tag{7}$$

where E_{np} represents the band gap of the NPs, mo is the rest mass of electron, m^*_e is the effective mass of the electron (= 0.19 m_o), R is the radius of the particle, m^*_h is the effective mass of the hole (= 0.8 m_o), ε_r is dielectric constant (= 5.7), E_g is the band gap of bulk CdS (= 2.42 eV), ε_o is the permittivity of free face and e is the charge of the electron [20].

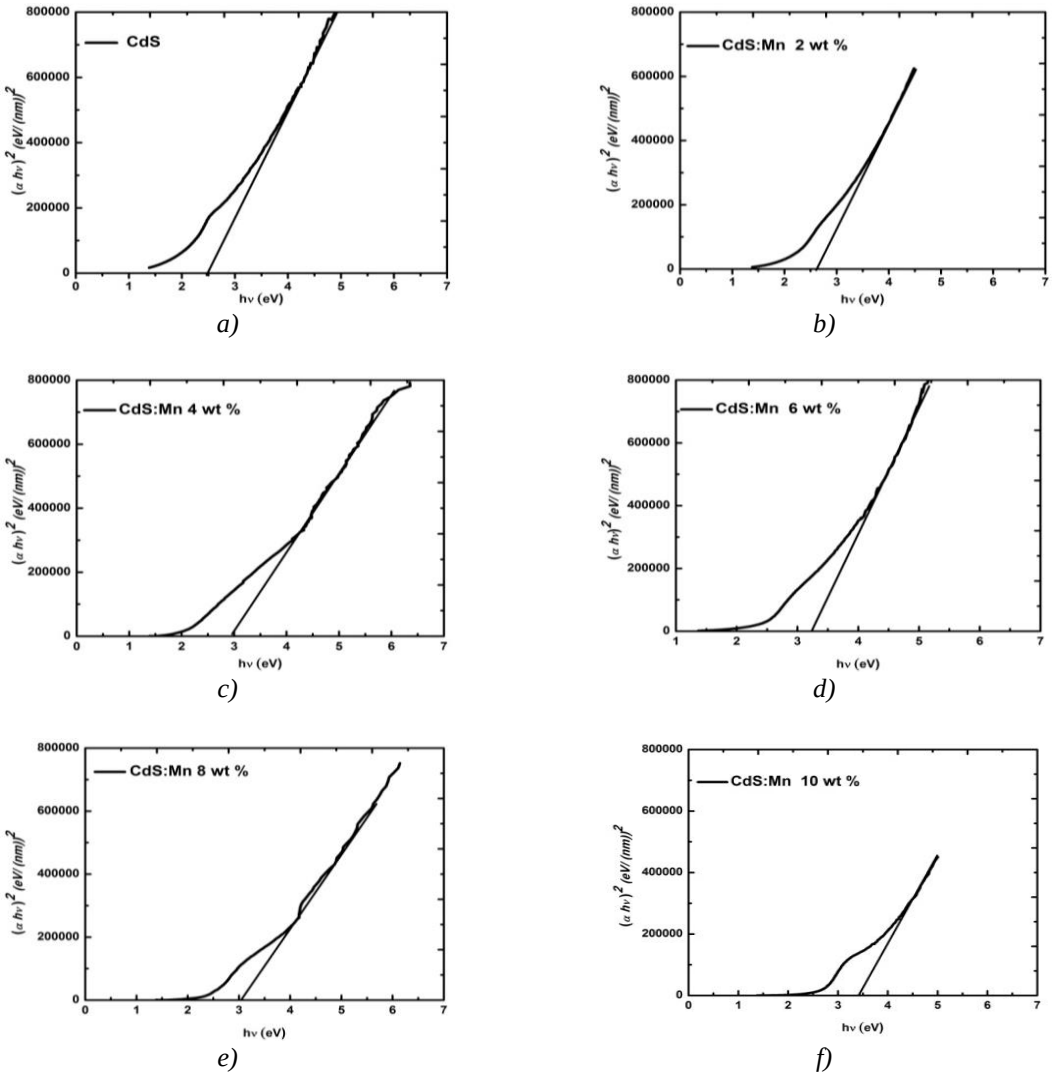

Fig. 8. Band gap spectra of a) CdS (b) CdS:Mn (2 wt %), (c) CdS:Mn (4 wt %), (d) CdS:Mn (6 wt %), (e) CdS:Mn (8 wt %) and (f) CdS:Mn (10 wt %).

The calculated particle size obtained from Brus formula of undoped and Mn doped CdS NPs (2, 4, 6, 8, & 10 wt %) found to be 7.91, 6.52, 3, 5.23, 4.65, 4.07 and 3.72 nm respectively. The calculated size of given prepared samples corresponding to the absorption spectra are shown in Table 3.

Table 3 the calculated size of the prepared NPs corresponding to absorption edge using Brus's. Eq.

Samp. Code	*Samp. Type*	*Abs. edge (nm)*	*Energy gap eV*	*UV–Vis Av. Part. size (nm)*
S1	CdS	504	2.5	7.91
S2	CdS:Mn (2 wt %)	477	2.6	6.52
S3	CdS:Mn (4 wt %)	449	3	5.23
S4	CdS:Mn (6 wt %)	435	3.2	4.65
S5	CdS:Mn (8 wt %)	420	3.1	4.07
S6	CdS:Mn (10 wt %)	410	3.4	3.72

Photoluminescence Studies

The photoluminescence (PL) emission is one of the most important physical properties in CdS NPs. PL emission related to shape, synthesis conditions, size and energetic position of the surface states [11-13]. The fluorescence spectra were measured by using a fluorescence spectrometer JASCO-FP-6300 (at excitation wavelength 350 nm).

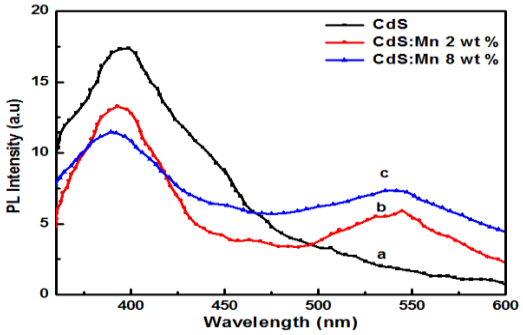

Fig. 9. Photoluminescence spectra for a) CdS, (b) CdS:Mn (2 wt %) and (c) CdS:Mn (8 wt %).

The PL emission spectra for undoped and Mn doped CdS NPs (2, & 8 wt %) is shown in Figure 9. PL spectra of aqueous surfactant solution without NPs were recorded and showed no emission at same excitation. This result indicates that the photo physical properties of CdS nanoparticles depend up on the size and surface passivation. The peaks are broad, indicating the formation of nanoparticles. For undoped CdS sample, a broad peak centered at 410 nm is observed when excited with 350 nm radiation. The characteristic emission peak observed for the CdS phase nanoparticles lies in the visible region of 400 nm – 520 nm. The peaks centered near at 410 nm correspond to the band gap or near band gap emission originates from recombination of electron hole pairs. For Mn doped CdS NPs (2, & 8 wt %) samples, new peak appear around 550 nm and the characteristic emission peak for the CdS showed a slightly blue shift as compared to undoped CdS sample. The peak at 550 nm originates from transition between $^4T_1$ excited state and the $^6A_1$ ground state of the Mn^{+2} ions inside a nanocrystalline CdS lattice. The last discussion confirms the incorporation of Mn in the CdS lattice. From XRD studies, as a result of confinement effect; the particle size was decreased with the increasing of Mn concentration. Although the blue shift of the emission peak related to the decrease of the particle size and presence of the surface defects that can lead to the collection of positive charges at the defect sites caused by Mn ions [14, 23]. Figure 10 shows the schematic energy diagram which explains the emission mechanism of CdS:Mn NPs.

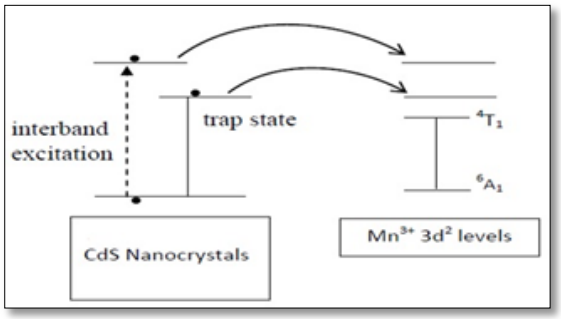

Fig. 10 Schematic diagram of the excitation of Mn^{+2} in CdS nanocrystals.

Table 4 Variation in emission peak for pure and Mn doped CdS nanoparticles.

Sample code	*Samples*	*1st emission peak (nm)*	*2nd emission peak (nm)*
S1	Pure CdS	410	----
S2	CdS doped 2 % Mn	405	550
S5	CdS doped 8 % Mn	400	550

Table 4 shows the variation in photoluminescence peak with wavelength for S1,S2 and S5. This variation in peak energy may be attributed to surface defects [15].

3.4. Magnetic Properties

Fig. 11 shows the magnetic hysteresis (M–H) loops at RT for the undoped and Mn doped CdS NPs (2, 6 & 8 wt %). For undoped CdS, the plot demonstrates that pure CdS is intrinsic diamagnetic response with negative slopes. The diamagnetism behavior in pure CdS NPs has been attributed to the fact that d-electrons are completely paired. Mn doped CdS NPs (2, 6 &8 wt %) demonstrate superparamagnetic (paramagnetic with weak ferromagnetic) behavior at room temperature.

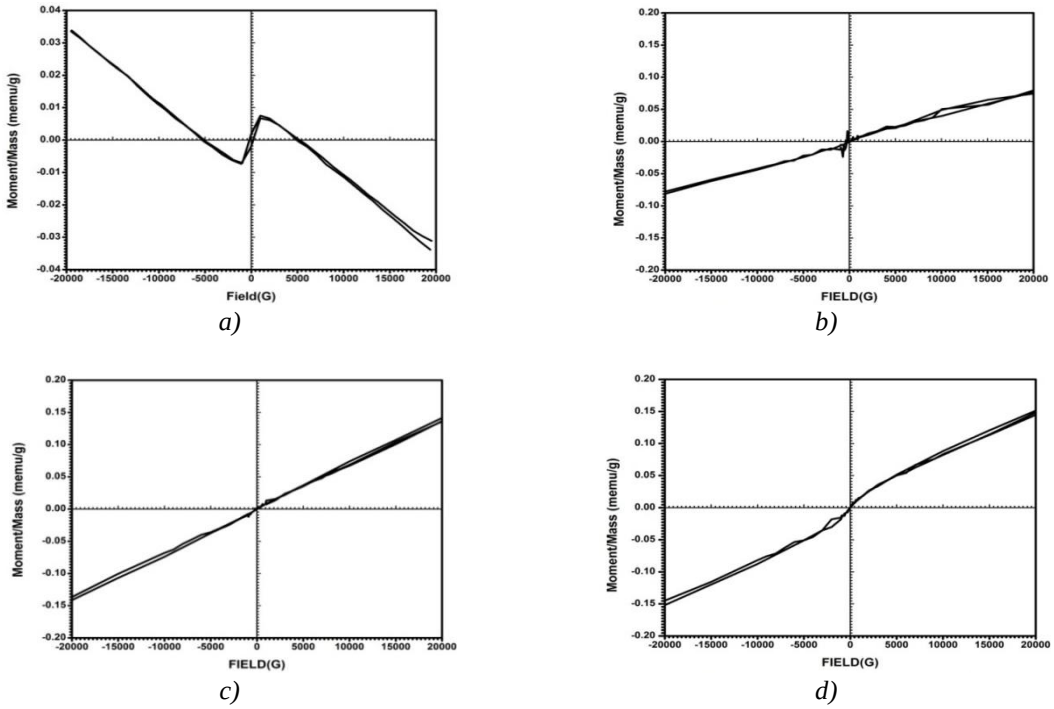

Fig. 11. (M–H) plots at RT for a) CdS, (b) CdS:Mn (2 wt %), (d) CdS:Mn (6 wt %) and (d) CdS:Mn (8 wt %).

The resultant magnetic properties depend on synthetic methodologies, concentration, and site occupation, size of quantum dots, or cluster, and shape of the host materials. [16]. Also, the magnetic properties of the prepared CdS:Mn samples depend on the magnitude of the transition metal (TM) ion exchange coupling with the electronic levels. The cubic zinc blende structure for CdS:Mn differ significantly with the bond structures between the magnetic ion and its Next-Nearest-Neighbour (NNN) cations.

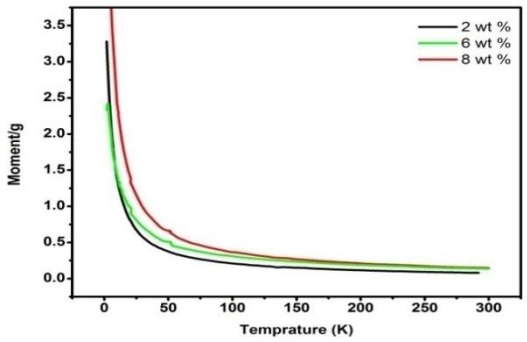

Fig. 12. M−T plots of undoped and Mn doped CdS (2, 6, & 8 wt %) NPs

Fig. 12 shows the (M–T) curves were also measured at temperature range of (20–300 K) for Mn doped CdS NPs (2, 6 & 8 wt %). The plot shows that, the magnetization is almost constant in the temperature range of (300–50 K) followed by a sudden increase upon further cooling toward 20 K. There is a difficult to determine the exact value of Curie temperature as its value is exceeding the range of our measurements. The Similar behavior has been reported [26].

4. Conclusion

Nanoparticles of undoped and manganese doped cadmium sulfide (CdS:Mn) with varying weight percentage 2, 4, 6, 8 and 10 % have been synthesized by wet chemical reaction route using mercaptoethanol (ME) as capping agent. Multiple techniques like XRD, EDX, HRTEM, UV-vis spectroscopy, Pl and VSM are used to study the structure, morphology, optical and magnetic properties of the prepared CdS:Mn NPs. XRD informed the cubic structure of the pure and Mn doped CdS samples. The average crystallite size is ranged from ~ 4 to ~7 nm. The purity and Mn concentration on the prepared samples has been confirmed by EDX analysis. The optical studies revealed that, the absorption spectra of the prepared samples exhibited varying blue shifts in their characteristic absorption wavelength edge as a function of Mn concentration. The sizes are estimated from X-ray diffraction by Debye-Scherer formula and compared with high resolution electron microscopy (HRTEM) and optical spectra. HRTEM images indicated that, the mean particle size are between 4.5-8 nm and exhibits polycrystalline behavior as observed from selected area electron diffraction (SAED) pattern. The optical band gap of the prepared samples increased from 2.5 to 3.4 eV with an increasing of Mn concentration because of the decreasing of the particle size. The recorded photoluminescence (PL) emission spectra at excitation of 350 nm depicted emission peaks occur at around 410 nm originates from recombination of electron hole pairs of CdS lattice. The peak at 550 nm from transition between $^4T_1$ excited state and the $^6A_1$ ground state of the Mn^{+2} ions. VSM data reveals diamagnetic behavior in undoped and superparamagnetic behavior (weak hysteresis loop) in Mn doped CdS samples at room temperature. The origin of magnetization has been discussed in this paper. All the prepared samples have semiconducting behavior and can be used in dilute magnetic semiconductor applications and fabrication of solar cells and light emitting diodes [17, 26-29].

References

[1] R. N. Bhargava, D. Gallagher, T. Welker, J. Lumin. **275**, 60 (1994).
[2] Ying Wang, N. Herron, J. Phys. Chem. **95**, 525 (1991).
[3] M. Ramrakhiani Piyush Vishwakarma, P. Singh, D.P. Bisen,The Open Nanoscience Journal **5**, 34 (2011).
[4] J. K. Furdyna, J. Appl. Phys. **64**, 29 (1988).

[5] S. Rite John, S. Florence, Chalcogenide Lett. **6**, 535 (2009).
[6] S. Rahman, K. Nadeem, M. A. Rehman, M. Mumtaz, S. Naeem, I. L. Papst, Ceram. Int. **39**, 5235 (2013).
[7] S. W. Yao, Y. X. Han, W. X. Liu, W. G. Zhang, H. Z. Wang, Mater.Chem. Phys. **101**, 247 (2007).
[8] M. Ethayaraja, C. Ravikumar, D. Muthukumaran, K. Dutta, R. Bandyopadhyaya, J. Phys. Chem. **111**, 3246 (2007).
[9] L. M. Qi, H. Colfen, M. Antonietti, Nano Lett. **1**, 61 (2001).
[10] L E Brus J. Chem. Phys. 79, 5566 (1983).
[11] W. Chen, Z.G. Wang, Z.J. Lin, L.Y. Lin, J. Appl. Phys. 82, 3111 (1997).
[12] T. Arai, T. Yoshida, T. Ogawa, J. Appl. Phys. **62**, 396 (1987).
[13] M. Agata, H. Kurase, S. Hayashi, K. Yamamoto, Solid State Commun. **76**, 1061 (1990).
[14] P. H. Borse, N. Deshmukh, R. F. Shinde, S. K. Date, S.K. Kulkarni, J. Mater. Sci. **34**, 6087 (1999).
[15] A. Lusson, J. Wagner, M. Ramsteiner Appl. Phys. Lett. **54**, 1787 (1989).
[16] A. Lewicki, A.I. Schindler, P.M. Shand, B.C. Crooker, J.K. Furdyna, Phys,Rev. B **44**, 6137 (1991).
[17] A. Gadala, M. S. Abd El-Sadek, R. Hamood, Chalcogenide Letters **14**, 239 (2017).
[18] Ruby Chauhan, Ashavani Kumar, Ram Pal Chaudhary, Res Chem Intermed **39**, 645 (2013).
[19] Jamil K. Salem, Talaat M. Hammad, S. Kuhn, Mohammed Abu Draaz, Naser K. Hejazy, R. Hempelmann, J Mater Sci: Mater Electron **25**, 2177 (2014).
[20] S Muruganandam, G Anbalagan, G Murugadoss, Indian J Phys **89**, 835 (2015).
[21] Nikita H. Patel, M.P. Deshpande, Sandip V. Bhatt, Kamakshi R. Patel, S. H. Chaki, Adv. Mat. Lett. **5**, 671 (2014).
[22] M. Thambidurai, N. Muthukumarasamy, S. Agilan, N. Sabari Arul, N. Murugan, R. Balasundaraprabhu, J Mater Sci **46**, 3200 (2011).
[23] A. K. Kole, P. Kumbhakar, Appl Nanosci **2**, 15 (2012).
[24] Jianing Zhao, Xiaoli Li, Zhiguo Li, Journal of Nanomaterials **2015**, (2015).
[25] M. KARMAKAR, O. MONDAL, B. ROY, P. K. PAUL, M. PAL, NANO: Brief Reports and Reviews **8**, 1350058 (2013).
[26] S.Aksu, E.Bacaksiz, M.Parlak, S.Yılmaz, I.Polat, M.Altunbaş, M.Türksoy, R.Topkaya, K.Özdoğane, Materials Chemistry and Physics **130**, 340 (2011).
[27] Hamed Rahimi, Ali Ghasemi, Reza Mozaffarinia, Majid Tavoosi, J Supercond Nov Magn **29**, 2041 (2016).
[28] VD Mote, Y Purushotham, BN Dole, Journal of Theoretical and Applied Physics **6**, 6 (2012).
[29] Raunak Kumar Tamrakar, Res Chem Intermed **41**, 43 (2015).